I&EC research
Industrial & Engineering Chemistry Research

Article

pubs.acs.org/IECR

Control Relevant Model of Amine Scrubbing for CO_2 Capture from Power Plants

Matthew S. Walters, Yu-Jeng Lin, Darshan J. Sachde, Thomas F. Edgar, and Gary T. Rochelle*

McKetta Department of Chemical Engineering, The University of Texas at Austin, Austin, Texas 78712, United States

Supporting Information

ABSTRACT: A low-order amine scrubbing model was developed for an intercooled absorber and advanced flash stripper configuration with piperazine solvent. The low-order lumped parameter model uses semi-empirical thermodynamics and rate-based mass transfer and embeds reaction kinetics in a constant overall transfer coefficient. The predicted off-design steady state of this model is compared to a high-order Aspen Plus simulation for 100−85% power plant load. The difference in CO_2 removal rate between the two models is less than 1% when power plant load is greater than 94%. The removal rate is systematically overpredicted in the low-order model because a constant CO_2 mass transfer coefficient in the absorber leads to an overprediction of absorber performance at part-load operation. Compared to pilot plant data, the low-order model captures the dynamic response of a step change in the stripper pressure control valve. The characteristic time of the total CO_2 inventory is found to be 77 min, compared to a total liquid residence time of 48 min. The low-order model sufficiently represents process behavior and will be used in future work to screen regulatory process control strategies.

INTRODUCTION

Post-combustion amine scrubbing is a leading technology for carbon capture from coal-fired power plants.[1−4] A basic overview of the process is shown in Figure 1, including the absorber, stripper, and multistage CO_2 compressor. Developing a dynamic model for the system is necessary to understand the effects of disturbances on process operation and for controller design. A low-order model of an advanced amine scrubbing process using aqueous piperazine (PZ) is formulated in this work. A small number of adjustable parameters in the model help account for uncertainties. The intent of this low-order model is to capture the general behavior of the process for screening regulatory control strategies; a high-order model is required for rigorous process design and optimization studies.[5]

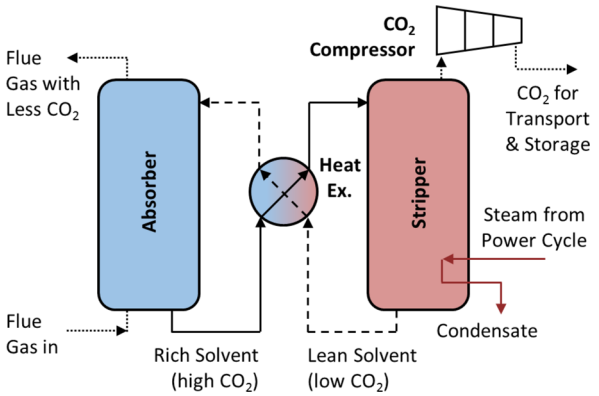

Figure 1. Basic flowsheet of an amine scrubbing plant.

Previous Research. There are limited examples of equation-based plantwide dynamic models of post-combustion amine scrubbing in the literature. Ziaii-Fashami[6] developed a dynamic model of the absorber/stripper process in Aspen Custom Modeler for a 100 MWe coal-fired power plant but did not perform any validation to quantify model performance. Enaasen Flø et al.[7] implemented a dynamic pilot plant model in MATLAB and performed both steady state and dynamic model validation. Nittaya et al.[8] created a model in gPROMS for capture from a 750 MWe coal-fired power plant. The absorber from this model was validated using steady state pilot plant data in previous work.[9] Lawal et al.[10] presented a dynamic model formulation that was implemented in gPROMS to simulate a pilot plant scale system, as well as a full-scale 500 MWe coal-fired power plant. The pilot-scale model was validated with steady state pilot plant data. Ceccarelli et al.[11] used Process System Enterprise's proprietary gCCS package in gPROMS to capture CO_2 from a 350 MWe NGCC plant but did not provide any model validation. All of the previous research presented here used monoethanolamine (MEA) as the solvent with the basic process configuration shown in Figure 1. The next section discusses the simplifications made in the low-order formulation of this work and compares it to previously published equation-based plantwide dynamic models.

Motivation and Objectives. A robust low-order dynamic model can be a useful tool for screening studies, sensitivity analyses, and model-based control. However, it must first be proved that the low-order model is capable of representing the process to have confidence in the model results. The validation study performed in this work uses two distinct data sets. The first is a steady state high-order Aspen Plus model. This model used hundreds of laboratory data points to regress 43 thermodynamic parameters for the $PZ/H_2O/CO_2$ system and has been extensively validated with pilot plant results.[5] The

Received: November 19, 2015
Revised: January 14, 2016
Accepted: January 25, 2016
Published: January 25, 2016

DOI: 10.1021/acs.iecr.5b04379
Ind. Eng. Chem. Res. 2016, 55, 1690−1700

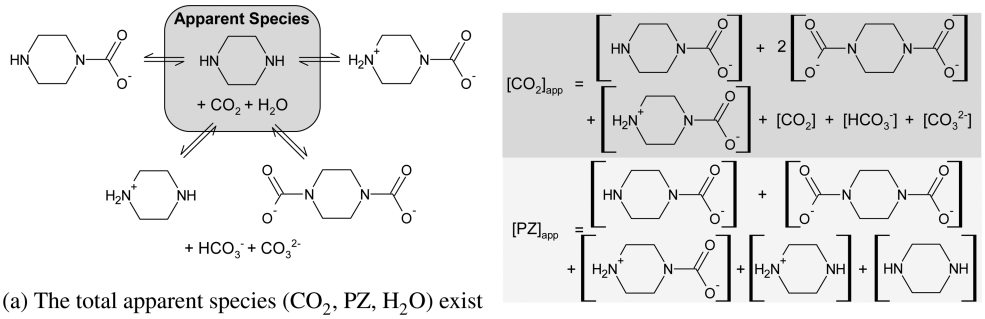

(a) The total apparent species (CO_2, PZ, H_2O) exist as true species in an electrolyte solution

(b) Apparent concentration of CO_2 and PZ

Figure 2. True versus apparent species representation.

second is dynamic pilot plant data produced from an open-loop step change experiment. The dynamic pilot plant experiment allows the model to be validated during transient conditions. This work examines the accuracy and limits of the low-order model through the validation activity and also uses the model to explore the residence time of the total CO_2 inventory in the process.

FIRST-PRINCIPLES MODELING OF AMINE SCRUBBING

There are five fundamental model components necessary to create a plantwide amine scrubbing model (either steady state or dynamic): flow type, thermodynamics, transport, kinetics, and contactor and exchanger characteristics. The following discussion briefly reviews the various levels of complexity with which these properties can be incorporated into the overall model and specifies how they are used in the low-order model of this work.

Flow Type. Flow type refers to how the bulk properties of a fluid are calculated along the spatial dimension of the flow in columns or heat exchangers. Discretized partial differential equations represent a plug flow regime in a distributed model, while a lumped model uses ordinary differential equations at one or more well-mixed nodes to approximate the distributed system.[12] Equations 1a and 1b show a liquid side mole balance on component i for structured packing using distributed and lumped models, respectively:

$$\frac{\partial(\varepsilon C_i^{\mathrm{L}})}{\partial t} = -\left(\frac{4}{\pi D^2}\right)\frac{\partial(x_i F^{\mathrm{L}})}{\partial Z} + N_i, \qquad Z/L \in [0, 1) \tag{1a}$$

$$\frac{d(\varepsilon C_{i,k}^{\mathrm{L}})}{\mathrm{d}t} = \left(\frac{4N_s}{\pi D^2 L}\right)(x_{i,k-1}F_{k-1}^{\mathrm{L}} - x_{i,k}F_k^{\mathrm{L}}) + N_{i,k}, \qquad \forall\ k \tag{1b}$$

where C is molar concentration, D is column diameter, F is molar flow rate, L is total length of the packing, N is volume-specific interphase molar transfer rate, N_s is the total number of well-mixed stages, x is liquid mole fraction, Z is the axial dimension, ε is liquid hold-up, superscript L refers to the liquid phase, and subscript k refers to the stage number. As $N_s \rightarrow \infty$, the lumped model approaches the distributed model. A lumped formulation with a small value for N_s is used in the low-order model.

Thermodynamics. Electrolyte activity coefficient models[13] are the recommended thermodynamic method to rigorously predict vapor−liquid equilibrium (VLE) of a CO_2−amine−water system.[14] This approach requires all true ionic species present in solution to be defined in the model. Figure 2 describes the difference between true and apparent species representations. Alternatively, a simplified semi-empirical model (eq 2) was developed by Xu[15] to calculate CO_2 VLE using the concentration of the apparent species in solution:

$$\ln(P_{\mathrm{CO2}}^{*}) = c_1 + c_2\frac{1}{T} + c_3\alpha + c_4\alpha^2 + c_5\frac{\alpha}{T} + c_6\frac{\alpha^2}{T} \tag{2}$$

where P_i^* is the equilibrium partial pressure, T is temperature, α is loading defined as moles CO_2/moles alkalinity, and c is a constant. The accompanying VLE relation for water (eq 3), based on Raoult's Law, assumes no free CO_2 exists in solution:

$$P_{\mathrm{H2O}}^{*} = \frac{x_{\mathrm{H2O}}}{1 - x_{\mathrm{CO2}}}P_{\mathrm{H2O}}^{\mathrm{sat}}(T) \tag{3}$$

where $P_{\mathrm{H2O}}^{\mathrm{sat}}$ is the saturation pressure of water at a given T.

In a thermodynamically consistent model, the heat of absorption of CO_2 (ΔH_{CO2}) and heat capacity of the loaded solution ($C_{\mathrm{p}}^{\mathrm{L}}$) should be related to the VLE.[16,17] To simplify the calculation, ΔH_{CO2} and $C_{\mathrm{p}}^{\mathrm{L}}$ are treated as constants that can be adjusted to account for uncertainty in the energy balance.

Material and Energy Transport. CO_2 absorption and desorption is known to be a mass-transfer limited process and, therefore, must be modeled using rate-based nonequilibrium equations.[18] The most sophisticated model for calculating multicomponent mass transfer through a two-film boundary layer is Maxwell−Stefan diffusion.[19] The Maxwell−Stefan equations require binary diffusion coefficients for all species and therefore the true speciation must be known.

A simpler approach uses two-film resistance theory with an apparent species mass transfer coefficient. The amine can be assumed to be nonvolatile ($N_{\mathrm{Am}} = 0$) and O_2 and N_2 in the flue gas can assumed to be insoluble (N_{O2}, $N_{\mathrm{N2}} = 0$) without significantly affecting the overall process dynamics. In general, there are $N_{\mathrm{comp}} - 1$ independent flux equations, where N_{comp} is the number of components. It is valid to assume negligible bulk convection and write N_{comp} independent flux equations in the cases of (1) low total flux, (2) presence of an inert in high concentration, or (3) equimolar counterdiffusion. Because the absorber gas is mostly insoluble N_2 and O_2 (case 2), the assumption holds in the absorber column. The stripper does not fall into any of the three cases for the negligible bulk convection assumption to be valid; however, negligible bulk convection has nevertheless been assumed in the low-order model to avoid solving a highly nonlinear system of equations. The two-film equations with apparent species mass transfer coefficients are given in eqs 4a−4d:

DOI: 10.1021/acs.iecr.5b04379
Ind. Eng. Chem. Res. 2016, 55, 1690−1700

$$N_{i,k}^{L} = V_k k_{l,i} a(x_{i,k}^{I} - x_{i,k}) \quad (4a)$$

$$N_{i,k}^{V} = V_k k_{g,i} a(P_{i,k} - P_{i,k}^{I}) \quad (4b)$$

$$N_{i,k}^{L} + r_{i,k} = N_{i,k}^{V} = N_{i,k} \quad (4c)$$

$$y_k^{I} = f(x_k^{I}, T_k^{I}, P) \quad (4d)$$

where a is specific interfacial area, k_g and k_l are gas and liquid film apparent mass transfer coefficients, N^V and N^L are transfer rates through the vapor and liquid films, P is total pressure, r is reaction rate, V is volume, and superscript I refers to the gas/liquid interface. These equations assume that the gas/liquid interface (1) has no accumulation (eq 4c) and (2) is at equilibrium (eq 4d). In the most general case, the mass transfer coefficients are a function of the apparent diffusion coefficient, temperature, fluid velocity, and packing geometry. In the low-order model, the mass transfer coefficients are treated as constant, adjustable parameters.

Interphase energy transfer occurs as a result of two phenomena: enthalpy transfer from interphase material flux and natural convection due to a temperature gradient. Because the thermal conductivity of the liquid is much greater than that of the gas, the low-order model assumes that there is no temperature gradient in the liquid film ($T_k^L = T_k^I$). The interphase energy transport (N_H) is determined by eq 5:

$$N_{H,k} = V_k h_k^{V} a(T_k^{V} - T_k^{L}) + N_{T,k}\hat{H}_k^{V} \quad (5)$$

where $\hat{H}$ is specific enthalpy and h is the convective heat transfer coefficient. h is related to the gas mass transfer coefficient for water through the Chilton−Colburn analogy; however, it is treated as an independent parameter in the low-order model.

Kinetics. Low-temperature CO_2 absorption is further limited by reaction kinetics occurring in the liquid film, which can be explicitly modeled using the Arrhenius equation for calculating reaction rate or implicitly modeled as an enhancement to the apparent mass-transfer coefficient. The parameter k_g' has been defined[20] to account for the enhancement due to chemical reaction of the apparent CO_2 liquid film mass transfer coefficient. This parameter is measurable experimentally, unlike a true enhancement factor, and is mostly a function of CO_2 loading.

The entire resistance to mass transfer across the two-film boundary (K_g) is calculated using a series resistance model (eq 6a), and the total interphase flux is determined based on a partial pressure driving force between the bulk gas and bulk liquid (eq 6b):

$$\frac{1}{K_g} = \frac{1}{k_g} + \frac{1}{k_g'} \quad (6a)$$

$$N_i = VK_{g,i} a(P_i - P_i^{*}) \quad (6b)$$

where P_i is partial pressure of the bulk vapor. K_g is treated as an adjustable parameter in the low-order model. Figure 3 summarizes the physical and chemical resistances occurring in the boundary layer.

Contactor and Exchanger Characteristics. The type of packing used in the absorber and stripper affects mass and heat transfer coefficients as well as hydraulic properties. Similarly, heat exchanger design is important for calculating the overall heat transfer coefficient and hydraulics. In general, the transfer coefficients, liquid hold-up, and pressure drop are functions of geometry and fluid velocity; in the low-order model it is assumed these parameters are constant at their design point.

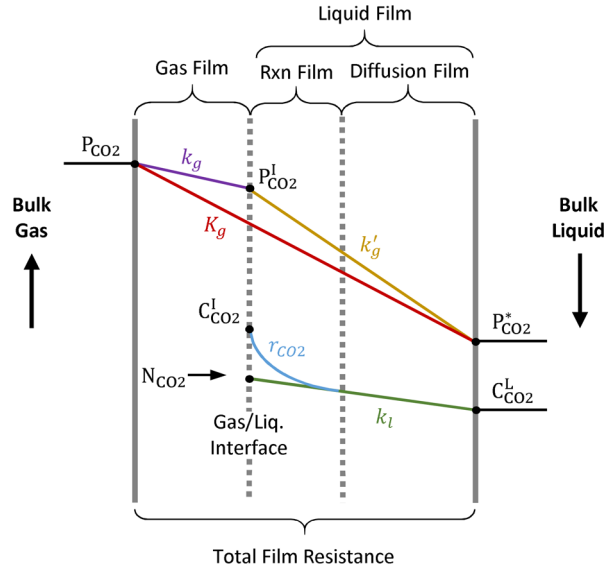

Figure 3. Physical and chemical resistances occurring in the boundary layer. In the gas film, there is physical resistance to mass transfer (k_g). The liquid film has both physical resistance (k_l) and a rate-limited chemical reaction (r). The liquid resistances are lumped into the parameter k_g'. The total two-film resistance is lumped into the parameter K_g.

Summary of Model Complexity. Table 1 assigns the model parameters discussed in the preceding sections into high-, medium-, and low-order models. The groupings attempt to pair model properties that have approximately equivalent levels of complexity.

Table 2 summarizes the characteristics of previously published plantwide dynamic models. Based on these characteristics, an overall level of model order is assigned according to the guidelines in Table 1.

Table 2 shows that there are currently no published high-order plantwide dynamic models, which include rate-based mass transfer with explicit reactions occurring in the liquid film. The discretized film reactions cause high-order models to be difficult to initialize and not robust in off-design conditions, making them unsuitable for dynamic simulation of disturbances and set point changes.

■ ADVANCED PROCESS FLOWSHEET

The plantwide dynamic amine scrubbing models listed in Table 2 use the baseline solvent MEA with a simple absorber and reboiled stripper configuration. Because of the high capital cost and large energy penalty associated with CO_2 capture, a commercial plant will likely use an advanced solvent with an intensified process. Here we model an in-and-out intercooled absorber with the advanced flash stripper (Figure 4) using aqueous PZ solvent, which is more representative of expected system performance than MEA with a simple absorber and reboiled stripper. PZ is an attractive solvent candidate because it can be regenerated at a high temperature and high pressure, has a fast reaction rate, and is resistant to degradation and corrosion.[21] Absorber intercooling reduces the required solvent flow rate and height of structured packing by decreasing the temperature bulge in the column that results from the

DOI: 10.1021/acs.iecr.5b04379
Ind. Eng. Chem. Res. 2016, 55, 1690−1700

Table 1. Overview of Model Complexity

	high-order	medium-order	low-order
flow type	distributed (plug flow)	distributed (plug flow)	lumped (well-mixed)
thermo	activity-based (true species)	activity-based (true species)	semi-empirical (apparent species)
transport	rate-based (Maxwell–Stefan)	rate-based (variable apparent k_g and k_l)	rate-based (constant apparent K_g)
kinetics	reactions in discretized liquid film	embedded in variable apparent k'_g	embedded in constant apparent K_g
contactor characteristics	variable hydraulics (geometry and velocity dependent)	variable hydraulics (geometry and velocity dependent)	constant hydraulics (fixed at design point)

Table 2. Previously Published Equation-Based Plantwide Dynamic Models

	model type	thermo	transport	kinetics	overall order
Ziaii-Fashami (2012)[6]	lumped	semi-empirical	rate-based	embedded in k'_g	medium
Enaasen Flø et al. (2015)[7]	distributed	semi-empirical	rate-based	enhancement factor	medium
Nittaya et al. (2014)[8]	distributed	semi-empirical	rate-based	enhancement factor	medium
Lawal et al. (2012)[10]	distributed	e-NRTL	rate-based	instantaneous reaction	low
Ceccarelli et al. (2014)[11]	distributed	gSAFT	rate-based	instantaneous reaction	low
this work	lumped	semi-empirical	rate-based	embedded in K_g	low

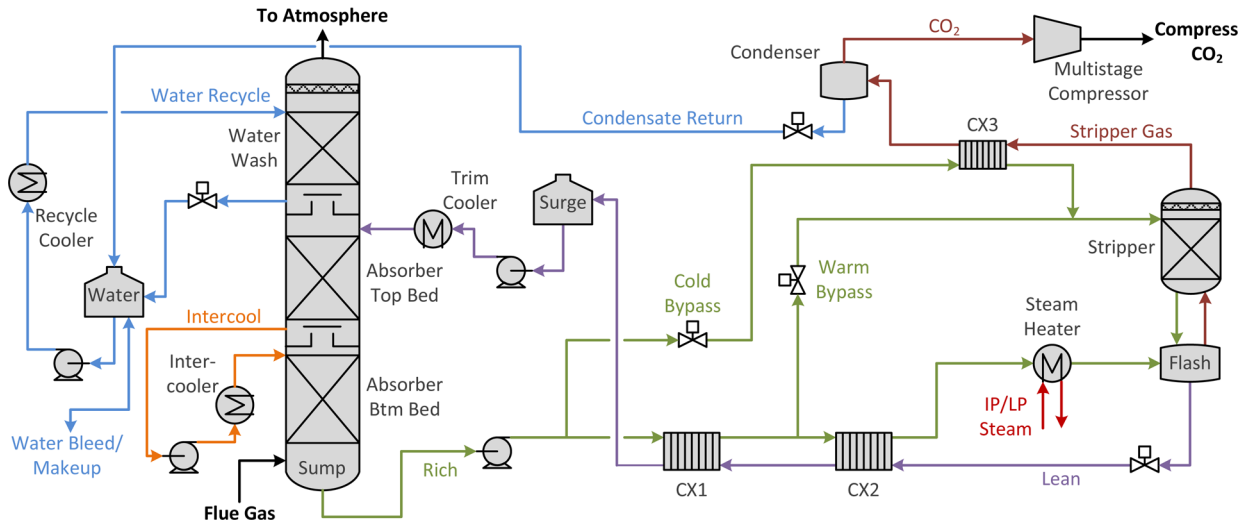

Figure 4. In-and-out intercooled absorber with advanced flash stripper configuration.

exothermic absorption of CO_2.[22] Finally, the energy performance of the advanced flash stripper configuration is superior to a reboiled stripper due to the effective recovery of stripping steam heat.[23]

The dynamic equations for the low-order model of the process shown in Figure 4 are given in the Supporting Information. The model was implemented in MATLAB and solved using ODE15s.

MODEL VALIDATION

Steady State Off-Design Validation with High-Order Model. The first objective of the low-order model validation activity was to quantify the model performance as the system moves away from its design point. The off-design steady state solutions of the model should be sufficiently accurate to predict energy performance and general plant behavior. Here we compare the off-design steady state solutions of the low-order model to a rigorous and previously validated high-order model.

Case Study. The system was designed to handle flue gas from a 550 MWe coal-fired power plant specified by Case 11 of NETL (2010).[24] The flue gas conditions for the 100% load case are given in the Supporting Information. It is assumed that the flue gas was passed through a direct contact cooler before entering the absorber to cool it to 40 °C. This model makes no restrictions on the availability of steam extracted from the power cycle for CO_2 regeneration. The flow rate of CO_2 out of the condensate tank is set by a multistage compressor, and it is assumed that the compressor can always achieve the specified flow.

High-Order Aspen Plus Model. A high-order Aspen Plus model[5] was previously used to design the process in Figure 4 for this case study.[25] The high-order model was simulated for a range of off-design power plant loads to compare to the low-order model. In each off-design case, the following conditions were maintained:

- Constant L/G ratio in the absorber of 4.32 kg/kg
- 5 molal PZ entering the absorber
- Constant c_{CX} in the equation $UA = c_{CX}F_{avg}^{0.7}$ for the main cross exchangers, where F_{avg} is the average molar flow rate of the hot and cold sides of the exchanger and c_{CX} is fit for both exchangers to give the correct LMTD at the design point
- Constant UA for the overhead vapor exchanger
- No H_2O accumulation or depletion in the system by adjusting the water wash recycle flow rate

DOI: 10.1021/acs.iecr.5b04379
Ind. Eng. Chem. Res. 2016, 55, 1690–1700

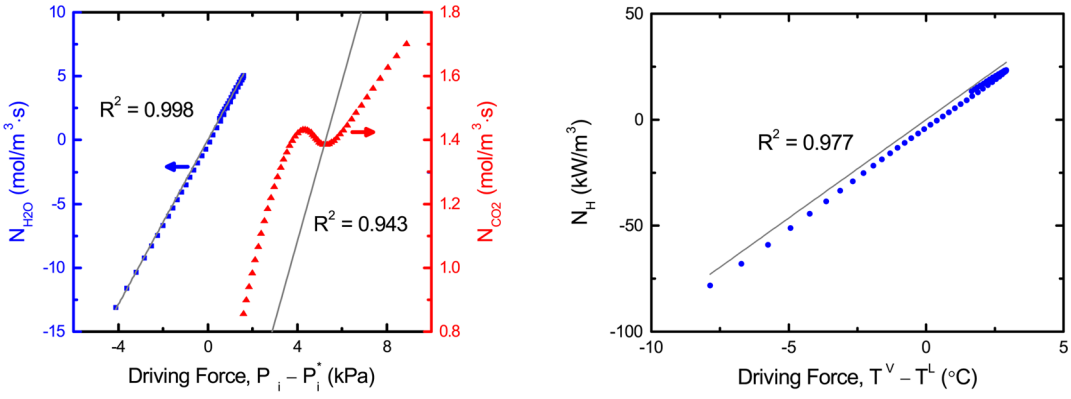

(a) Molar transfer rates (b) Energy transfer rate

Figure 5. Transfer rates versus driving force for the absorber top bed predicted by high-order Aspen Plus model, using Sulzer 250X packing and a lean loading of 0.22.

- 90% CO_2 removal by adjusting lean loading into the absorber
- Constant flash tank temperature by adjusting the heat duty
- Constant cold and warm bypass ratios of 9% and 35%, respectively
- Lean loading target for the absorber met by adjusting the flash tank pressure

The overall mass and heat transfer coefficients in the absorber, water wash, and stripper used in the Aspen Plus simulation were found by plotting the transfer rate against the driving force predicted by the high-order model for each bed of packing and determining the slope. Figure 5 demonstrates this procedure for the absorber top bed of packing. Table 3 summarizes the transfer coefficients found for the packed sections within the system. While there is a good fit for the heat transfer coefficient and the mass transfer coefficient of H_2O, there is clearly uncertainty in the CO_2 mass transfer coefficient. The nonlinear behavior in the CO_2 transfer profile occurred because the temperature bulge from the exothermic absorption of CO_2 affected the reaction kinetics. The maximum liquid temperature of 60.4 °C for the absorber top bed of packing was observed at a CO_2 partial pressure driving force of 5.1 kPa, which corresponds to the minimum in the CO_2 transfer rate profile.

Table 3. Overall Mass and Heat Transfer Coefficients for Packed Beds Fitted from Aspen Plus Model

	$K_{g,CO2}a$ (mol/kPa·m³·s)		$K_{g,H2O}a$ (mol/kPa·m³·s)		ha (kW/m³·s)	
	value	R^2	value	R^2	value	R^2
absorber top bed	0.29	0.943	3.2	0.998	9.3	0.977
absorber btm bed	0.11	0.926	2.9	0.972	9.2	0.957
stripper	0.12	0.871	1.2	0.969	13.0	0.998
water wash			4.2	1.000	7.1	0.999

Heat exchanger overall transfer coefficients (UA) are given in the Supporting Information. These coefficients were set by specifying a LMTD of 7.7 and 7.0 °C on the two main exchangers (CX1 and CX2, respectively) and a LMTD of 20 °C on the overhead vapor exchanger (CX3).

The nonvolatile amine assumption was examined using the high-order model. Figure 6 plots the PZ vapor fraction for a range of possible flash tank operating conditions. The vapor fraction was well under 1% for design case, as well as for any off-design condition that might reasonably occur.

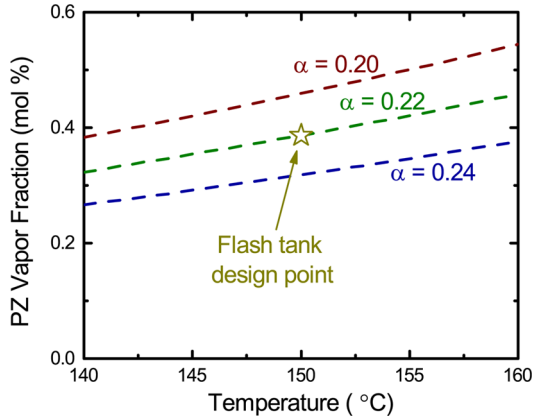

Figure 6. Vapor fraction of PZ predicted by high-order model for a range of temperatures and lean loadings (α).

Adjusted Parameters. Several parameters were adjusted in the low-order MATLAB model to match the design conditions from the high-order Aspen Plus model. The normalized squared error between the low-order model and design case was minimized to adjust the parameters simultaneously in each section of the system (absorber side, stripper side, and entire plant), as summarized in Table 4. The table shows that seven physically significant parameters were used to match seven experimentally measurable target values from the design case only; a nonlinear parameter estimation using data from a range of power plant loads was not performed.

Table 4. Adjusted Parameters in Low-Order Model

	adjusted parameter	target
absorber	$K_{g,CO2}a$	CO_2 removal
	C_p^V	T_{out}^V flue gas
stripper	ΔH_{CO2}, ΔH_{H2O}	flash tank T and P
	$K_{g,CO2}a$	CO_2 stripping rate
	C_p^V	T_{out}^V stripper gas
plantwide	C_p^L	$Q_{CX1,hot} = Q_{CX1,cold}$

DOI: 10.1021/acs.iecr.5b04379
Ind. Eng. Chem. Res. 2016, 55, 1690−1700

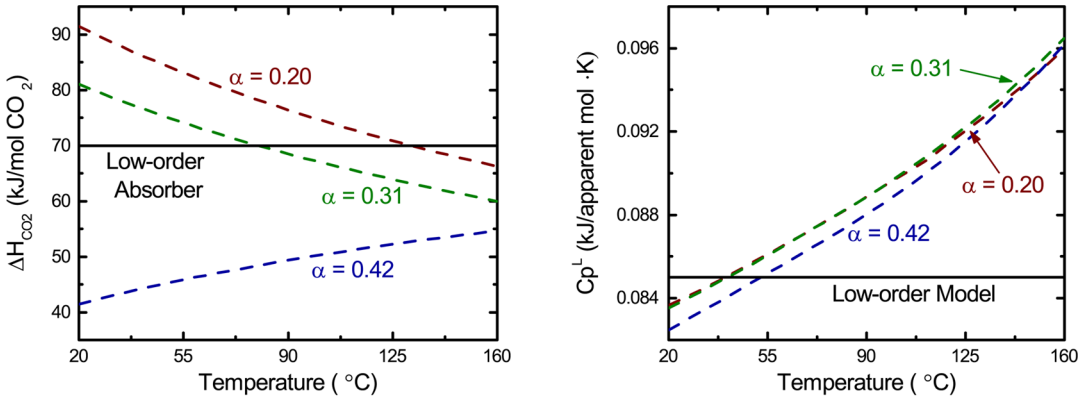

Figure 7. Constant thermodynamic parameters from the low-order model (solid) compared to values predicted by the thermodynamically consistent high-order Aspen Plus model for a range of temperatures and loadings.

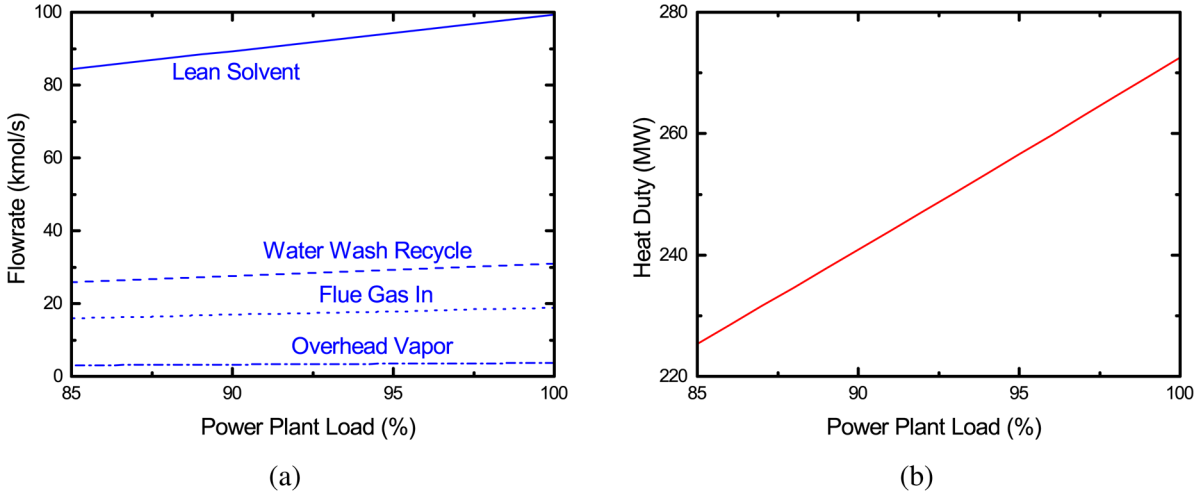

Figure 8. Inputs to low-order MATLAB model calculated from high-order Aspen Plus simulation.

To match the 90% CO_2 removal rate at design conditions, $K_{g,CO2}a$ was allowed to vary by ±20%. The ratio of the overall CO_2 mass transfer coefficient for the top and bottom absorber beds was kept constant, according to eq 7:

$$\frac{K_{g,CO2,top}}{K_{g,CO2,btm}} = \left(\frac{K_{g,CO2,top}}{K_{g,CO2,btm}}\right)_{old} \quad (7)$$

where the subscript old denotes the value from Table 3. The values used in the low-order model are given in the Supporting Information.

The nominal values for ΔH_{CO2} and ΔH_{H2O} were assumed in the absorber. To match the VLE on the stripping side of the process, these values were varied by ±20%. C_p^L was calculated based on the performance of CX1 and C_p^V was set to match the outlet temperature of the absorber or stripper gas. The thermodynamic parameters are listed in the Supporting Information. Figure 7 compares the constant solvent thermodynamic parameters of the low-order model to a range of values predicted by the thermodynamically consistent high-order model.

Results from Boiler Load Reduction. Partial-load (100–85%) operation of the coal-fired power plant was examined, assuming that the inlet flow rate of flue gas is be directly proportional to load and the flue gas CO_2 concentration is constant. Figure 8 gives the inputs to the low-order model based on the results from the high-order model. Figure 9 shows that the low-order model is well-behaved near the design load.

Dynamic Validation with Pilot Plant Data. The second objective of the low-order model validation is to show that it captures the general behavior of the process dynamics. In order to have confidence in a control system designed using the low-order model, the model should accurately represent the major time constants present in the system. The dynamic response of the model was compared to pilot plant data to quantify its ability to predict the characteristic time of the total CO_2 inventory in the system.

Separations Research Program Pilot Plant. While a growing body of steady-state amine scrubbing pilot plant data is available for model validation, dynamic data are relatively scarce. Enaasen Flø et al.[7] have previously performed a dynamic model validation that used data from the Gløshaugen pilot plant. The Separations Research Program (SRP) at the University of Texas at Austin has an amine scrubbing pilot plant that uses synthetic flue gas equivalent to a 0.1 MWe coal-fired power plant.[26] The pilot plant is configured similar to Figure 4 but does not contain a water wash section of the absorber or a compressor. The amine solvent is nominally 5 molal PZ. In the Spring 2015 SRP campaign, dynamic step tests

DOI: 10.1021/acs.iecr.5b04379
Ind. Eng. Chem. Res. 2016, 55, 1690–1700

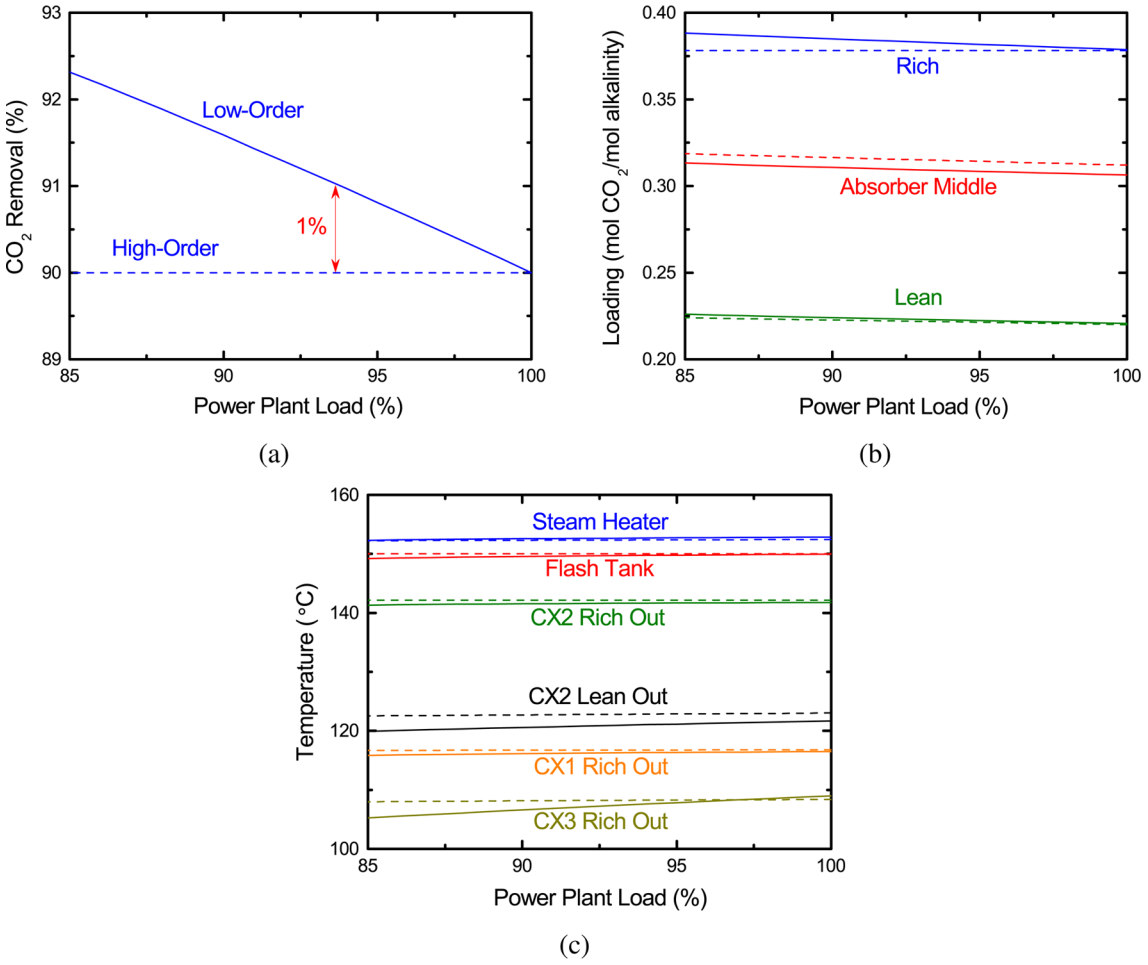

Figure 9. Validation of low-order MATLAB model with high-order Aspen Plus model.

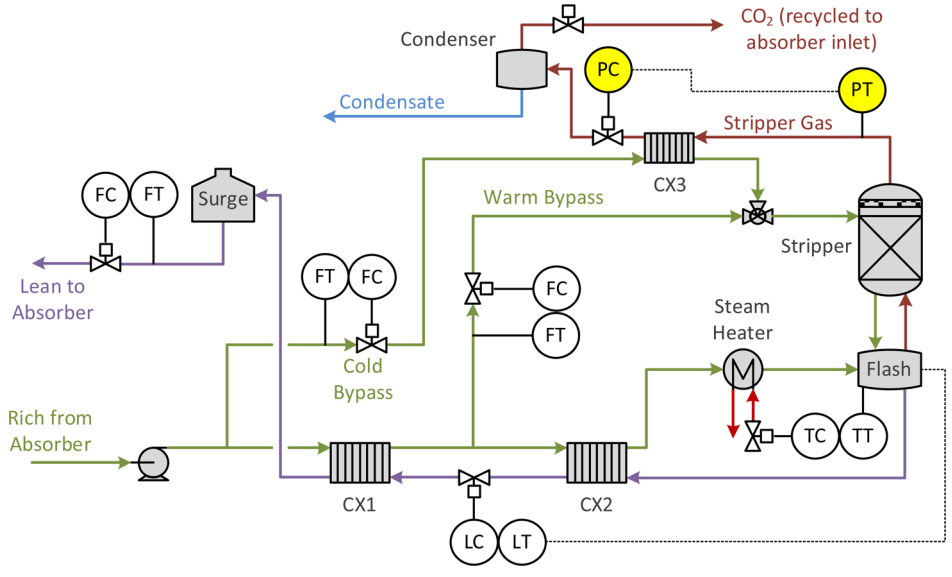

Figure 10. SRP pilot plant control system.

were completed to acquire meaningful data which can be easily interpreted and used to validate a dynamic model.

An experiment was performed to test the dynamics of the total CO_2 inventory of the system. When the desired steady state was reached, the stripper pressure control valve in Figure 10 was switched from automatic to manual. A step change was made in the valve position, which effectively changed the flow rate of stripped CO_2 out of the process. An increase in valve position, corresponding to a decrease in stripper pressure, was selected for safety considerations to ensure the pressure ratings on the process equipment would not be exceeded. A relatively modest increase in valve position was made to avoid flooding

DOI: 10.1021/acs.iecr.5b04379
Ind. Eng. Chem. Res. 2016, 55, 1690−1700

the stripper or loosing control of the level in the flash tank. When the step change occurred, the stripper pressure immediately decreased, CO_2 was flashed out of the solvent at a faster rate, and the temperature of the flash tank decreased. Due to the nonaggressive tuning of the temperature controller on the flash tank, there was a slow ramp up in heat duty after the step change as the controller attempts to maintain the temperature set point. As the system began to approach steady state, the heat duty ramped back down.

Figure 11 shows the inputs to the dynamic model to simulate the step change. The heat duty reported in Figure 11 is a

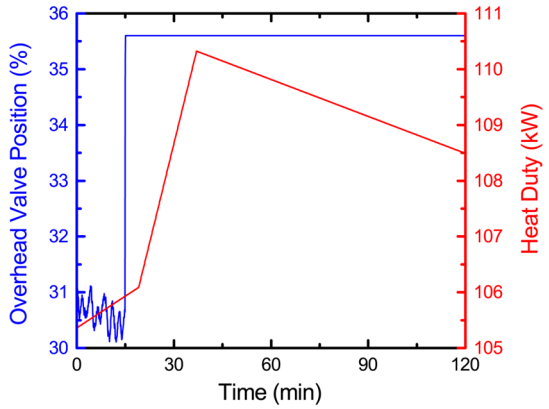

Figure 11. Inputs to model.

filtered signal, so the noise has been eliminated. It is assumed the inlet conditions to the absorber, all controlled levels, and all controlled flows remained constant during the dynamic test. The values of the constant inputs to the low-order model can be found in the Supporting Information.

The pressure control valve is an equal percentage valve, and it is operating at choked conditions as a result of the downstream condenser being at approximately atmospheric pressure. The flow rate through the valve can therefore be modeled according to eq 8, which contains constants that have been fitted to the pilot plant data:

$$F_{CO2}[\mathrm{kg/s}] = (9.66 \times 10^{-5})(29.51)^{q_v - 1} (P[\mathrm{Pa}])\sqrt{\rho^{V}[\mathrm{kg/m^3}]} \quad (8)$$

where q_v is the stem position of the valve (between 0 and 1) and ρ^V is the gas density at the valve inlet. Equation 8 assumes that condensed water that is in the two-phase flow leaving the hot side of CX3 has no effect on the CO_2 flow rate through the pressure control valve. Equation 8 predicts the measured CO_2 flow rate within 5% for 20 out of 21 steady state runs with varying conditions (Figure 12).

Several model parameters were adjusted to match the pilot plant data at steady state before the step change occurs. To achieve the desired removal and stripping rates, the CO_2 mass transfer coefficients were adjusted (Table 5). The change from the high-order values from the absorber are in good agreement with a previous pilot plant data reconciliation using the high-order Aspen Plus model, where the interfacial area in the absorber was adjusted by a factor of 0.74.[26] *UA* values were also calculated for pilot plant conditions and are given in the Supporting Information. All of the thermodynamic values from high-order model validation remained the same for the pilot plant validation.

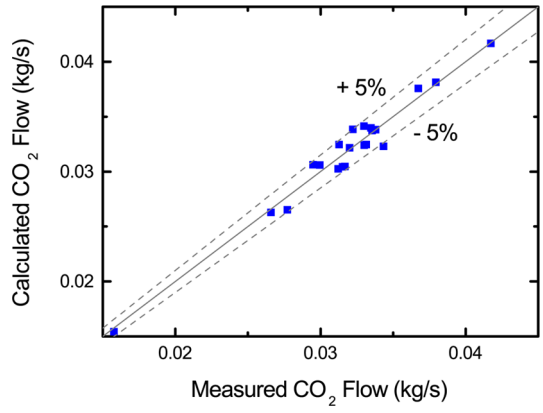

Figure 12. Stripper overhead CO_2 flow rate parity plot for stripper gas conditions of 4−7 bar and 8−18 °C.

Table 5. Fitted $K_{g,CO2}a$ (mol/kPa·m^3·s) for Packed Sections

	fit from high-order	fit from SRP	$\frac{K_{g,CO2}a\mathrm{SRP}}{K_{g,CO2}a\mathrm{HighOrder}}$
top bed	0.339	0.253	0.744
bottom bed	0.125	0.094	
stripper	0.128	0.128	1.00

Results from Open-Loop Step Test. After 15 min of steady state operation, the stripper overhead valve was placed in manual and a 5% step change increase was made to the position of the valve (Figure 11). Density, which is measured online, was used to quantify the changes in lean and rich loadings over time. The Freeman density equation[27] was used to calculate the density predicted by the low-order model at a given loading. This density was normalized by the density of water at the predicted temperature to remove the temperature dependence on density. The calculated value was compared to the measured value, which was normalized by the density of water at the temperature measured by the densitometer. Figure 13 compares the model response with the measured dynamics. The SRP data in Figure 13 were sampled at a rate of 5 s from the lean stream at a flow rate of 10 gpm and from the cold rich stream at a flow rate of 0.5 gpm.

Transport delay from piping is ignored in the low-order model, leading to the delay between the predicted and measured lean density response shown in Figure 13a. This delay does not significantly impact the overall response. As previously mentioned, nonaggressive tuning on the flash tank temperature controller caused a slow response in the heat duty supplied to the steam heater. This recovery back to the temperature set point is reflected as an increase in lean density both in the model and experimental data. Figure 13b shows that there is an initial small increase in the rich density immediately after the step change is made. This is likely an artificial effect caused by recycling the stripped CO_2 back to the absorber inlet in pilot plant operation. Imperfect flow control of the absorber inlet gas caused an increase in CO_2 concentration; in the true process this will not occur since the inlet flue gas composition is set by the upstream power plant. This change in inlet gas conditions is not captured by the low-order model, causing an offset between the measured and predicted rich density. The shape of the two curves, however, is the same. There is a time delay of approximately 15 min in the response of the rich loading in the low-order model, which largely reflects the capacity of the lean surge tank and absorber. The

DOI: 10.1021/acs.iecr.5b04379
Ind. Eng. Chem. Res. 2016, 55, 1690−1700

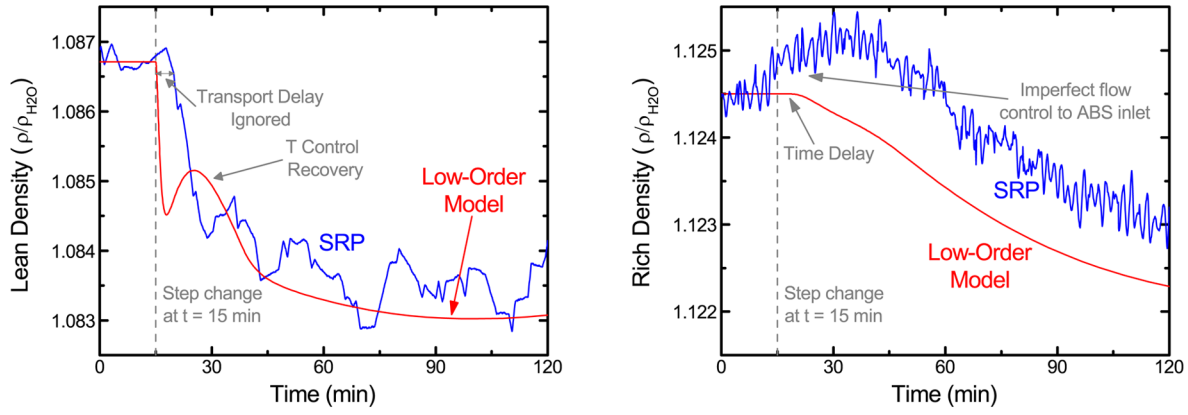

(a) Lean density (b) Rich density

Figure 13. Dynamic response to a step change in the overhead valve position.

increase in the measured signal begins to level off after 15 min, which is consistent with the time delay predicted by the model.

DISCUSSION

The CO_2 removal rate (Figure 9a) is the most important indicator of model performance since maintaining a removal target is likely the primary control objective of the process. The high- and low-order model removal rates agree within 1% when the power plant load is within 6% of the design case. This is sufficient for screening a regulatory control structure where disturbances in a base-loaded power plant are expected to be small. While the lean loading of the low-order model closely tracks the Aspen Plus simulation, rich loading is overpredicted as the power plant load decreases (Figure 9b). This indicates the absorber performance is being overpredicted, and that the decrease in the overall CO_2 mass transfer coefficient with decreasing fluid velocity is significant. This observation is consistent with the systematically high removal rate prediction. The predicted temperatures (Figure 9c) are in good agreement, showing a small number of adjustable thermodynamic parameters are sufficient. The rich side exchanger temperatures for the main cross exchanger with constant *UA* tracks the temperatures predicted using a *UA* which depends on fluid flow rate. Therefore, it can be concluded that constant *UA* is a good assumption at part-load when operating near the design case. For all cases, the low-order MATLAB model converged when given a set of set of initial conditions that were near the steady state solution; the high-order Aspen Plus model requires multiple initialization steps for convergence.

Processes with material and energy recycle are known to complicate process dynamics and control compared to cascaded units without recycle.[28,29] In the amine scrubbing system, the recycled lean solvent causes positive feedback in the absorber and increases the system time constant. Processes with heavy material recycle have historically included surge tanks to buffer disturbances at the expense of added capital cost and increased total inventory. The SRP pilot plant includes a large lean surge tank prior to the inlet to the absorber. The time constant for the CO_2 removal rate is associated with the total CO_2 inventory, most of which is in the lean surge tank. In the step change experiment, the rich loading time constant is representative of the total inventory. The pilot plant was not allowed to run to steady state after the step change occurred. However, simulating the model to steady-state in Figure 14 (by holding the heat duty at its final value in Figure 11) showed that the characteristic time of the CO_2 inventory is 77 min. This is much longer than the total liquid residence time of 47.7 min (Table 6) because of the significant material recycle from the stripper back to the absorber.

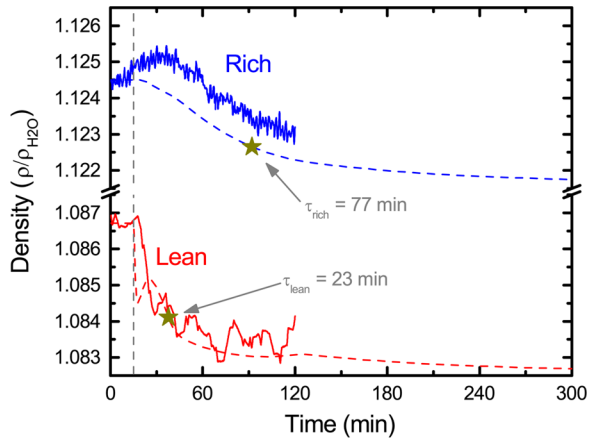

Figure 14. Characteristic times of density measurements.

Table 6. Liquid Residence Times for SRP Unit Operations

	residence time (min)
lean surge tank	37.5
absorber sump	2.7
CX1	2.1
flash tank	1.3
absorber chimney tray	1.3
CX2	1.3
absorber packing	1.1
absorber distributor	0.2
stripper packing	0.2
total	47.7

A commercial post-combustion capture plant will not be designed with a large surge tank because it increases safety risks by maintaining a large inventory of amine, presents operational challenges for solvents operating near their solid solubility limit, and is prohibitively expensive. A sensitivity analysis was performed with the low-order model by varying the hold-up of SRP solvent in the presence of the step change in overhead

DOI: 10.1021/acs.iecr.5b04379
Ind. Eng. Chem. Res. 2016, 55, 1690−1700

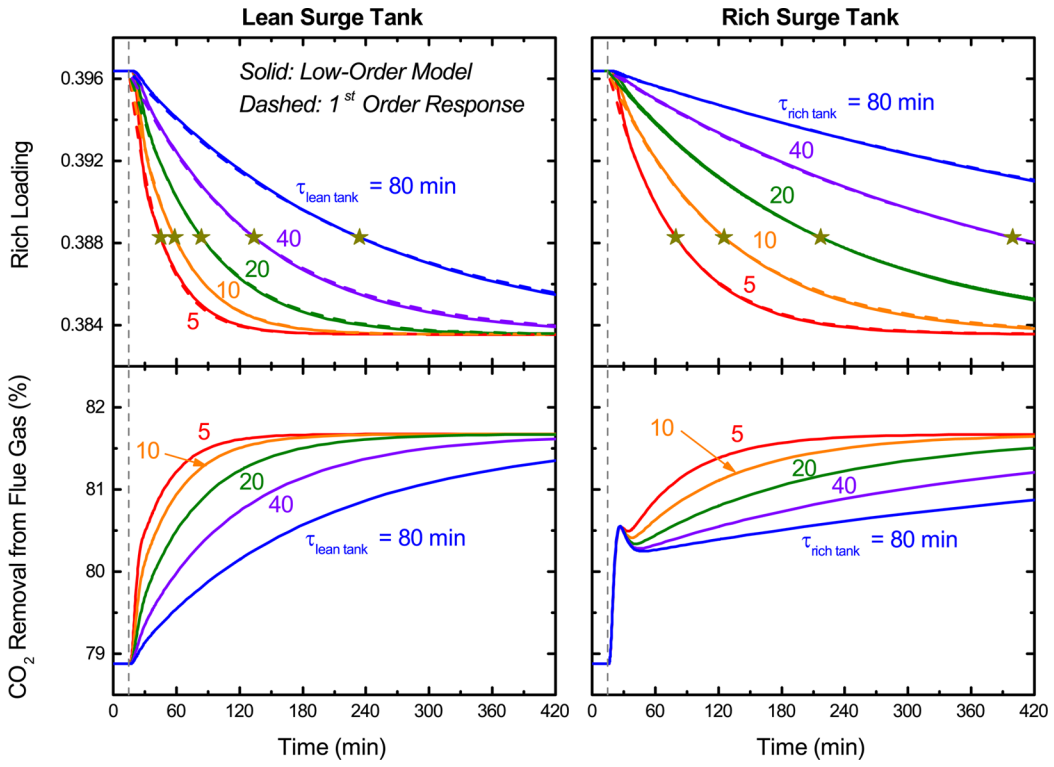

Figure 15. SRP surge tank sensitivity analysis showing the response of rich loading and CO_2 removal to a step change in overhead valve position predicted by the low-order model, with stars denoting the characteristic time of the response.

valve position, shown in Figure 15. All other residence times listed in Table 6 remained constant. To remove the dynamics associated with the varying heat duty, a step change was also made simultaneously to the steam heater duty to its final value in Figure 11. Both a lean surge tank and rich surge tank were considered. In the case of a rich surge tank, which was included as part of the absorber sump inventory for the simulation, the lean surge tank was given an initial level that corresponds to the original absorber sump inventory from Table 6.

The response of rich loading was compared to a first-order transfer function with the same gain and characteristic time, demonstrating that the rich loading displays a first-order response (top row of Figure 15). With a lean surge tank, the change in lean loading was buffered by the surge tank before it entered the absorber, causing a relatively slow initial response in CO_2 removal (bottom left of Figure 15). There was a fast initial response to CO_2 removal that tracked the lean loading in the case of a rich surge tank, followed by a slow approach to steady state as a result of feedback from the stripping side of the process (bottom right of Figure 15). Plotting the characteristic time versus the liquid residence time in Figure 16 shows that the slope was constant as the surge tank size was varied. In both lean and rich surge tank cases, the characteristic time was slower than the residence time. However, it was significantly slower in the case of a rich surge tank because there was a much larger inventory of CO_2 compared to the lean case. The slow characteristic time is important because it complicates tightly controlling the removal rate.

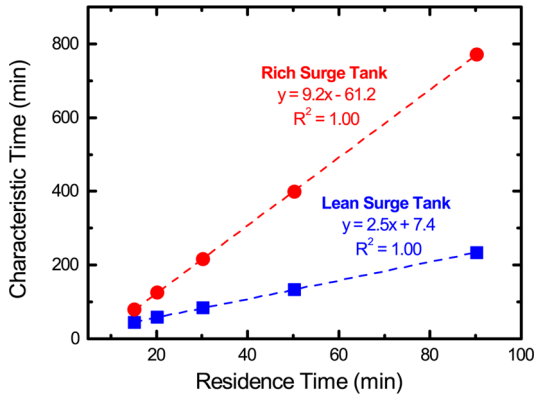

Figure 16. Dependence of the characteristic time of the rich loading on the total liquid residence time.

CONCLUSIONS

When compared to off-design steady state solutions of a high-order model, the low-order model is in good agreement near the design point. However, the low-order model systematically overpredicts absorber performance as the flue gas load decreases. The low-order model also correctly predicts the dynamic behavior of the overall CO_2 inventory when compared to SRP pilot plant data. Therefore, the low-order model presented here will be used in future work to design a regulatory control layer for the amine scrubbing process. Because of solvent recycle, the characteristic time of the pilot plant rich loading in response to a step change was 60% slower than the total liquid residence time. A sensitivity analysis showed that a lean surge tank causes a slow response in CO_2 removal from the flue gas, while a rich surge tank leads to a faster response in the absorber but a slower approach to steady state.

DOI: 10.1021/acs.iecr.5b04379
Ind. Eng. Chem. Res. 2016, 55, 1690−1700

■ ASSOCIATED CONTENT

Supporting Information

The Supporting Information is available free of charge on the ACS Publications website at DOI: 10.1021/acs.iecr.5b04379.

Low-order model equations, model parameters, and inputs (PDF)

■ AUTHOR INFORMATION

Corresponding Author

*E-mail: gtr@che.utexas.edu.

Notes

The authors declare the following competing financial interest(s): One author of this publication consults for Southern Company and for Neumann Systems Group on the development of amine scrubbing technology. The terms of this arrangement have been reviewed and approved by the University of Texas at Austin in accordance with its policy on objectivity in research. The authors have financial interests in intellectual property owned by the University of Texas at Austin that includes ideas reported in this paper.

■ ACKNOWLEDGMENTS

The authors acknowledge the financial support of the Texas Carbon Management Program and the University of Texas at Austin Cockrell School of Engineering Endowment.

■ REFERENCES

(1) Rochelle, G. T. Amine scrubbing for CO_2 capture. *Science* **2009**, *325*, 1652−1654.

(2) Rubin, E. S.; Mantripragada, H.; Marks, A.; Versteeg, P.; Kitchin, J. The outlook for improved carbon capture technology. *Prog. Energy Combust. Sci.* **2012**, *38*, 630−671.

(3) Stéphenne, K. Start-up of world's first commercial post-combustion coal fired CCS project: contribution of Shell Cansolv to SaskPower Boundary Dam ICCS Project. *Energy Procedia* **2014**, *63*, 6106−6110.

(4) Scherffius, J.; et al. Large-scale CO_2 capture demonstration plant using Fluor's Econamine FG^{SM} technology at NRG's WA Parish Electric Generating Station. *Energy Procedia* **2013**, *37*, 6553−6561.

(5) Frailie, P. T. Modeling of Carbon Dioxide Absorption/Stripping by Aqueous Methyldiethanolamine/Piperazine. PhD Dissertation, University of Texas at Austin, 2014.

(6) Ziaii-Fashami, S. Dynamic Modeling, Optimization, and Control of Monoethanolamine Scrubbing for CO_2 Capture. PhD Dissertation, University of Texas at Austin, 2012.

(7) Enaasen Flø, N.; Knuutila, H.; Kvamsdal, H. M.; Hillestad, M. Dynamic model validation of the post-combustion CO_2 absorption process. *Int. J. Greenhouse Gas Control* **2015**, *41*, 127−141.

(8) Nittaya, T.; Douglas, P. L.; Croiset, E.; Ricardez-Sandoval, L. A. Dynamic modeling and evaluation of an industrial-scale CO_2 capture plant using monoethanolamine absorption processes. *Ind. Eng. Chem. Res.* **2014**, *53*, 11411−11426.

(9) Harun, N.; Nittaya, T.; Douglas, P. L.; Croiset, E.; Ricardez-Sandoval, L. A. Dynamic simulation of MEA absorption processes for CO_2 capture from fossil fuel power plant. *Int. J. Greenhouse Gas Control* **2012**, *10*, 295−309.

(10) Lawal, A.; Wang, M.; Stephenson, P.; Obi, O. Demonstrating full-scale post-combustion CO_2 capture for coal-fired power plants through dynamic modelling and simulation. *Fuel* **2012**, *101*, 115−128.

(11) Ceccarelli, N.; van Leeuwen, M.; Wolf, T.; van Leeuwen, P.; van der Vaart, R.; Maas, W.; Ramos, A. Flexibility of low-CO_2 gas power plants: Integration of the CO_2 capture unit with CCGT operation. *Energy Procedia* **2014**, *63*, 1703−1726.

(12) Oh, M.; Pantelides, C. C. Combined lumped and distributed parameter systems. *Comput. Chem. Eng.* **1996**, *20*, 611−633.

(13) Chen, C.-C.; Britt, H. I.; Boston, J. F.; Evans, L. B. Local composition model for excess Gibbs energy of electrolyte systems. Part 1: Single solvent, single completely dissociated electrolyte systems. *AIChE J.* **1982**, *28*, 588−596.

(14) Austgen, D. M.; Rochelle, G. T.; Chen, C.-C.; Peng, X. Model of vapor-liquid equilibria for aqueous acid gas-alkanolamine systems using the electrolyte-NRTL equation. *Ind. Eng. Chem. Res.* **1989**, *28*, 1060−1073.

(15) Xu, Q. Thermodynamics of CO_2 Loaded Aqueous Amines. PhD Dissertation, University of Texas at Austin, 2011.

(16) Lewis, G. N.; Randall, M. *Themodynamics and the Free Energy of Chemical Substances*, 1st ed.; McGraw-Hill Book Company, Inc: New York, 1923.

(17) Mathias, P. M.; O'Connell, J. P. The Gibbs-Helmholtz equation and the thermodynamic consistency of chemical absorption data. *Ind. Eng. Chem. Res.* **2012**, *51*, 5090−5097.

(18) Taylor, R.; Krishna, R.; Kooijman, H. Modeling of distillation. *Chem. Eng. Prog.* **2003**, 28−39.

(19) Bird, R. B.; Stewart, W. E.; Lightfoot, E. N. *Transport Phenomena*, 2nd ed.; John Wiley & Sons, Inc.: New York, 2002.

(20) Dugas, R. E.; Rochelle, G. T. CO_2 absorption rate into concentrated aqueous monoethanolamine and piperazine. *J. Chem. Eng. Data* **2011**, *56*, 2187−2195.

(21) Rochelle, G.; Chen, E.; Freeman, S.; Van Wagener, D.; Xu, Q.; Voice, A. Aqueous piperazine as the new standard for CO_2 capture technology. *Chem. Eng. J.* **2011**, *171*, 725−733.

(22) Sachde, D.; Rochelle, G. T. Absorber intercooling configurations using aqueous piperazine for capture from sources with 4 to 27% CO_2. *Energy Procedia* **2014**, *63*, 1637−1656.

(23) Lin, Y.-J.; Madan, T.; Rochelle, G. T. Regeneration with rich bypass of aqueous piperazine and monoethanolamine for CO_2 capture. *Ind. Eng. Chem. Res.* **2014**, *53*, 4067−4074.

(24) NETL. *Cost and performance baseline for fossil energy plants, Volume 1: Bituminous coal and natural gas to electricity final report*, Revsion 2; 2010.

(25) Trimeric Corporation. *Techno-Economic Analysis for CO_2 Capture by Concentrated Piperazine with Regeneration by Advanced Flash Stripper Configuration: Budget Period 1*; 2015.

(26) Chen, E.; Madan, T.; Sachde, D.; Walters, M. S.; Nielsen, P.; Rochelle, G. T. Pilot plant results with piperazine. *Energy Procedia* **2013**, *37*, 1572−1583.

(27) Freeman, S. A. Thermal Degradation and Oxidation of Aqueous Piperazine for Carbon Dioxide Capture. PhD Dissertation, University of Texas at Austin, 2011.

(28) Luyben, W. L. Dynamics and control of recycle systems. 1. Simple open-loop and closed-loop systems. *Ind. Eng. Chem. Res.* **1993**, *32*, 466−475.

(29) Morud, J.; Skogestad, S. Dynamic behaviour of integrated plants. *J. Process Control* **1996**, *6*, 145−156.

DOI: 10.1021/acs.iecr.5b04379
Ind. Eng. Chem. Res. 2016, 55, 1690−1700